

Carbon Supported PtSn versus PtSnO₂ Catalysts in Methanol Oxidation

Sanja Stevanović^{1,*}, Dušan Tripković¹, Aleksandra Gavrilović-Wohlmuther², Jelena Rogan³,
Uroš Lačnjevac⁴, Vladislava Jovanović¹

¹ University of Belgrade - Institute of Chemistry, Technology and Metallurgy, Department of electrochemistry, Njegoševa 12, 11000 Belgrade, Republic of Serbia,

² Schoeller-Bleckmann Nitec GmbH, Hauptstrasse 2, 2630 Ternitz, Austria,

³ Faculty of Technology and Metallurgy, University of Belgrade, Karnrgijeva 4, 11000 Belgrade, Serbia,

⁴ Department of Material Science, Institute for Multidisciplinary Research, University of Belgrade, Kneza Višeslava 1, 11030 Belgrade, Serbia

*E-mail: sanjas@ihm.bg.ac.rs

Received: 6 November 2020 / Accepted: 21 December 2020 / Published: 31 December 2020

Pt, PtSn and PtSnO₂ catalysts supported on high surface area carbon synthesized by microwave assisted polyol procedure were tested for methanol oxidation. Based on TGA, EDX and XRD analysis, PtSn/C is composed of Pt and Pt₃Sn phase while the rest of Sn is present in a form of very small tin oxide particles. This paper focuses on structure-activity relationships for CO tolerance and methanol oxidation reactions after addition of Sn to Pt catalysts. Alloying of Sn with Pt improves the rate of CO oxidation despite the fact that the pure Sn does not react with CO and therefore activity for methanol oxidation increases ~ 2 times in comparison to Pt/C catalyst. PtSn/C catalyst shows small advantage in comparison with PtSnO₂/C catalyst due to the alloyed Sn and its electronic effect. Long term stability tests also confirmed that PtSn/C catalyst is somewhat better in comparison to PtSnO₂/C.

Keywords: platinum catalysts; microwave polyol synthesis; methanol oxidation; stability tests.

1. INTRODUCTION

Fuel cells as energy sources have a great advantage compared to fossil fuels and over the last few decades their technology has been actively researched and developed. Because energy derived from fossil fuels, especially in the transportation sector, has significant emissions of pollutants there are global concerns about how to overcome this problem. In addition to caring for the environment, fossil fuels are non-renewable energy sources and their resources in nature are limited.

Direct methanol fuel cells (DMFC) have great potential as power supplies for portable devices and transportation vehicles, recognized as one of the cleanest technologies for energy conversion [1]. The advantages of using DMFC are low working temperature, high efficiency and environmentally beneficial features. The key constraints for more successful DMFC commercialization are high production costs involving expensive metals, primarily platinum as well long-term degradation (especially detachment and agglomeration of the catalyst and consequential the reduction of active surface area).

Platinum-based catalysts are the most common investigated catalysts for methanol oxidation reaction [2,3]. Despite significant advances, high price of Pt is the most limiting factor for commercial utilization of DMFC. Over the past few years there has been enormous progress in the development of catalysts in which platinum is alloyed with cheaper metals such as Ru [3,4], Sn [5], Ni [5], Co [6], Au [7], etc. Among the most successful binary platinum catalysts for methanol oxidation reaction are PtSn and PtSnO₂. These catalysts are good choice since Sn is low-cost and easily available metal. The superior characteristics are reflected through a bi-functional mechanism and electronic effect. Studies report that presence of Sn activates water at much lower potential than Pt [8] and form hydroxyl adsorbed species (OH_{ads}) on catalysts surface. These OH_{ads} accelerate the removal of poisoning CO from the platinum sites. The promoting effect of Sn is also reflected in the modification of the electronic characteristics of the Pt leading to the reduction of the adsorption strength of strongly adsorbed species such as CO [9,10].

It is also well known that composition of bimetallic PtSn/C catalysts and alloying degree are important factors for catalysts activity. Toward to certain literature data, larger degree of alloying causes enlargement in activity for the PtSn/C catalysts [11]. However, insight in promoting effect of PtSnO₂/C catalyst, with Sn in non-alloyed oxidized form, is still not clarified. Literature data showing that the presence of SnO₂ in platinum catalysts could enhance the methanol oxidation reaction even in higher extent than PtSn catalyst. Ross founded that the successful removing of CO is dependent of SnO₂ instead of PtSn alloy phase [12]. In more recent studies it is suggested that non-alloyed SnO₂ in platinum catalysts can generate OH species at lower potential than Sn in alloyed phase [13]. It is also confirmed that addition of SnO₂ to platinum catalysts with carbon support can improve corrosion stability of the support [14]. On the other hand, Song et al. [15] observed a detrimental effect when Sn in oxidized form is present to a greater extent, probably due to its poor electronic conductivity.

Our examinations of PtSn/C catalyst revealed its high activity for the ethanol oxidation [16] and CO [17]. DFT modeling also showed that Sn either in alloyed or oxide form is responsible for increased oxidation rates for CO-like species [17].

Since it is still one of the most difficult factors to obtain the desired DMFC performance, the anodic oxidation reaction of the catalyst, this paper focuses on a detailed examination of methanol and CO electro-oxidation at an *as prepared* and electrochemically treated PtSn/C and PtSnO₂/C catalysts. The main goal of this work is to accentuate the potential of Sn loaded Pt catalysts for their practical applications in DMFC.

2. EXPERIMENTAL

Preparation of catalysts

Pt, PtSnO₂ and PtSn nanoparticles were synthesized by microwave assisted polyol procedure. In this procedure, 20 ml of ethylene glycol were mixed with 1 ml of 0.05 M H₂PtCl₆ alone or with 1 ml of SnCl₂ or 1 ml SnO₂ under magnetic stirring. SnO₂ nanoparticles were previously synthesized by microwave irradiation of SnCl₂ in ethylene glycol solution, for 60 s at 700 w. To adjust pH~12, 1 ml of 0.8 M NaOH was added dropwise. The prepared solutions were heated in microwave oven 60 s for the Pt, and 90 s for the PtSn and PtSnO₂ catalysts at 700 W. Obtained colloidal solutions were further mixed with 20 ml of water suspension of carbon (Vulcan XC-72R) and 150 ml 2 M H₂SO₄. The suspensions were filtered using vacuum pump and rinsed with high purity water (Milipure, 18 MΩ cm). The solid residues were dried at 160 °C in N₂ atmosphere for 3h. The metal loading for all catalysts was adjusted to ~20 mass %.

Characterization of the catalysts

Synthesized catalysts were analyzed by the thermogravimetric (TGA), differential thermal (DTA) and X-ray diffraction (XRD) characterization. These analyses were done under the same conditions as in our previous work [16]. Rietveld refinement procedure [18] with the structural parameters obtained from inorganic crystal structure database (ICSD): for Pt ICSD 03-065-2868 [19], PtSn ICSD 01-089-2056 [20], Pt₃Sn ICSD 03-065-0958 [21] and SnO₂ ICSD 01-071-5324 [22] were used. The average crystallite size and lattice parameters of each catalyst were calculated by Scherer formula [23]. The chemical composition of the samples was examined by scanning electron microscopy (SEM), while transmission electron microscopy (TEM) analysis was used for morphological tests. These techniques were also performed under the same conditions as in our previous work [16].

Electrochemical measurements

The electrochemical experiments were conducted in 0.1 M HClO₄ with a Pt wire as the counter electrode and a saturated calomel electrode (SCE) as reference one. However all the potentials are expressed versus reversible hydrogen electrode (RHE). Nafion-impregnated Pt/C, PtSn/C or PtSnO₂/C catalysts with the loading of 20 μg/cm² of the catalyst were deposited on the polished glassy carbon working electrode. The electrocatalytic activity of all catalysts was studied in 0.1 M HClO₄ + 0.5 M CH₃OH solution. The reaction was studied at Pt/C, PtSn/C and PtSnO₂/C catalysts in:

- as-prepared form (without any previous treatment) and
- oxide annealed form (obtained by cycling the potential up to 1.0 V vs SCE)

Catalyst stability was determined by chronoamperometric measurements and long-term potential cycling with setup conditions accepted in our previous work [16]. The electrochemical active surface area (EASA) was obtained from CO stripping voltammetry assuming the theoretical charge for

removal of CO monolayer is $420 \mu\text{C cm}^{-2}$. Catalysts activity is normalized with the respect to values obtained for the EASA.

3. RESULTS AND DISCUSSION

Characterization of the catalysts

TGA and DTA analyses revealed 20 wt.% for Pt/C, 18 wt.% for PtSn/C and 16 wt.% for PtSnO₂/C. EDX characterization of PtSn/C and PtSnO₂/C also showed certain difference from nominal (50:50) values. The Pt:Sn atomic ratios for PtSn/C is 58 at.% : 42 at.% while it is 68 at.% : 32 at.% for PtSnO₂/C catalyst. TEM analysis pointed similar particle size for all catalysts. TEM images with corresponding histograms are shown in Fig. 1. All particles for each catalyst are well distributed over high area carbon support and according to statistical analysis they are with rather similar diameter ranging from 2 to 3 nm.

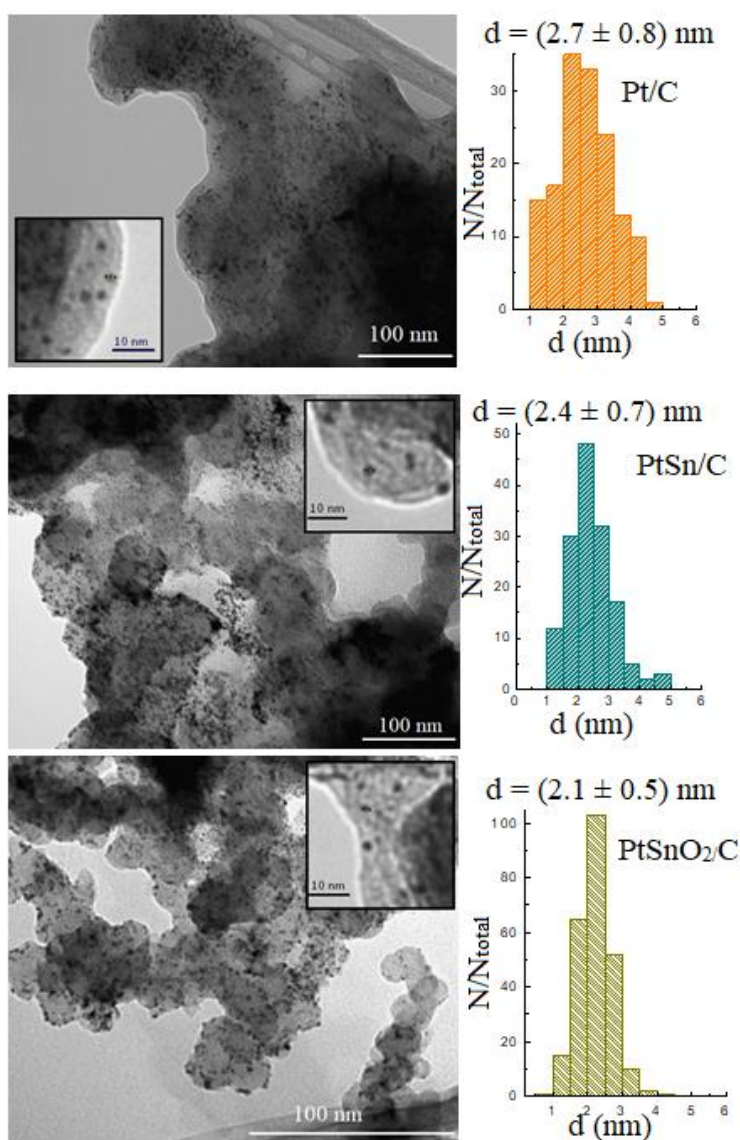


Figure 1. TEM image and particle size distribution of supported Pt/C, PtSn/C and PtSnO₂/C catalysts.

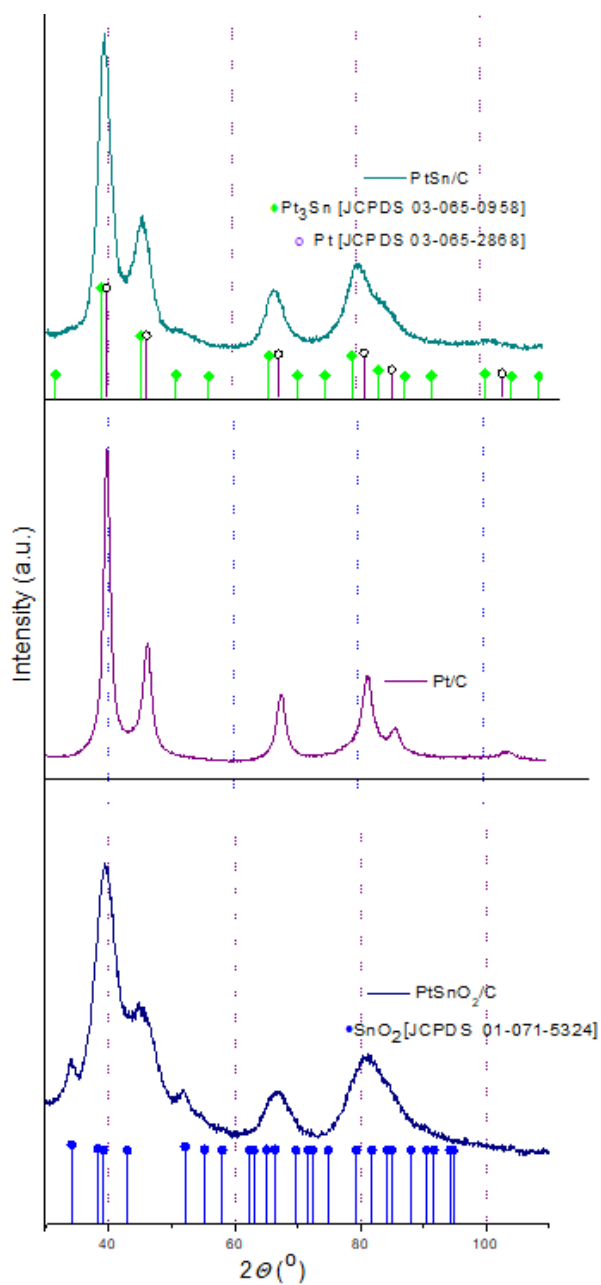


Figure 2. XRD patterns of supported Pt/C, PtSn/C and PtSnO₂/C catalysts.

The lattice parameters and particle size of all catalysts are summarized in Table 1.

Table 1. Lattice parameter and particle size for Pt/C, PtSn/C and PtSnO₂/C catalysts

Catalyst	Pt/C	PtSn/C	PtSnO ₂ /C
XRD Lattice parameter a (nm)	0.3921	Pt: 0.3924 Pt ₃ Sn: 0.3992	Pt: 0.3935 SnO ₂ : a=b=0.4713, c=0.3179
XRD Particle size (nm)	~ 3	Pt: ~ 2 nm Pt ₃ Sn: ~ 3	Pt: < 2 SnO ₂ : ~ 2

XRD analysis of all carbon-supported catalysts is presented in Figure 2. All diffraction patterns show characteristic peaks of face centered cubic (fcc) Pt crystalline structure. The position of the most intense line reflections for PtSn/C catalyst reveals two crystal phases: Pt and Pt₃Sn. The diffraction peaks for PtSn/C sample are slightly shifted to lower 2θ values with respect to the corresponding peaks for pure Pt in Pt/C sample, as a consequence of Pt-Sn alloy formation in addition to the Pt phase. This indicates that the addition of Sn to Pt, since Sn has bigger atomic radii than Pt ($R_{Pt} = 0.139 \text{ nm}$, $R_{Sn} = 0.14 \text{ nm}$), according to Vegard's law would induce extension of Pt lattice. As can be seen from the PtSn/C XRD patterns, incorporation of tin not only does lead to a shift of the peaks to lower 2θ values (compared to 2θ values for the fcc structure of Pt) but a second set of peaks exclusively characteristic for the presence of a fcc Pt₃Sn phase appears. Further, careful deconvolution of XRD peaks and calculations of the lattice parameters can give as information about tin and platinum atomic composition in the Pt-Sn alloy phases.. Two crystal phases are detected in the peak profile of PtSn/C: platinum (fcc - cubic system, space group Fm-3m) and Pt₃Sn (fcc - cubic system, space group Pm-3m). The obtained phase compositions using the Rietveld method show ~ 85% for Pt and ~ 15% for Pt₃Sn metal phases in PtSn / C. The calculated values reveals lattice constants for Pt and Pt₃Sn phases and they are 0.3924 and 0.3992 nm respectively. Two crystal phases were obtained in PtSnO₂/C catalyst: platinum (fcc - cubic system, space group Fm-3m) and SnO₂ (tetragonal, space group P42/mnm). In spite of the fact that peaks related to presence of Sn oxides in PtSn/C diffraction patterns are not observed, Sn oxide might exist as an amorphous phase or could not be detected because of too small crystallite size. This is also supported by data from TGA and EDX investigations which indicating negligible loss of the catalysts components and rather small percent of alloyed Sn. Moreover XPS and XRD analysis from the literature data, obtained for PtSn/C catalysts also prepared by microwave assisted polyol procedure pointed to the presence of Sn(0) and also considerable amount of Sn(IV) [24, 25]. Therefore, SnO₂ can actually be present in the PtSn/C catalyst, but as a result of its very small crystallite size cannot be detected by the XRD. Based on XRD analysis, the main difference of these two bi-metallic catalysts is the existence of a smaller quantity of Pt₃Sn alloy in the case of PtSn/C and no alloyed Sn but significantly larger SnO₂ particles in the case of PtSnO₂ catalyst. It can be also noticed that particle size obtained from XRD results is consistent with the results of TEM. The obtained small catalyst particles and the homogeneous particle size distribution clearly indicate the benefits of microwave synthesis.

Electrochemical performance of the catalysts

The electrochemical behavior of different catalysts was determined by cyclic voltammetry measurements. Since Sn dissolves at higher potentials (above 0.4 V vs SCE) [26], but at those potentials its oxide is stable [27], cyclic voltammetry measurements with and without methanol are performed at non-treated (as-prepared) as well as electrochemically treated (oxide annealed) PtSn/C and PtSnO₂/C catalysts. Basic cyclic voltammograms of all catalysts and cyclic voltammogram of carbon support are illustrated in Fig. 3.

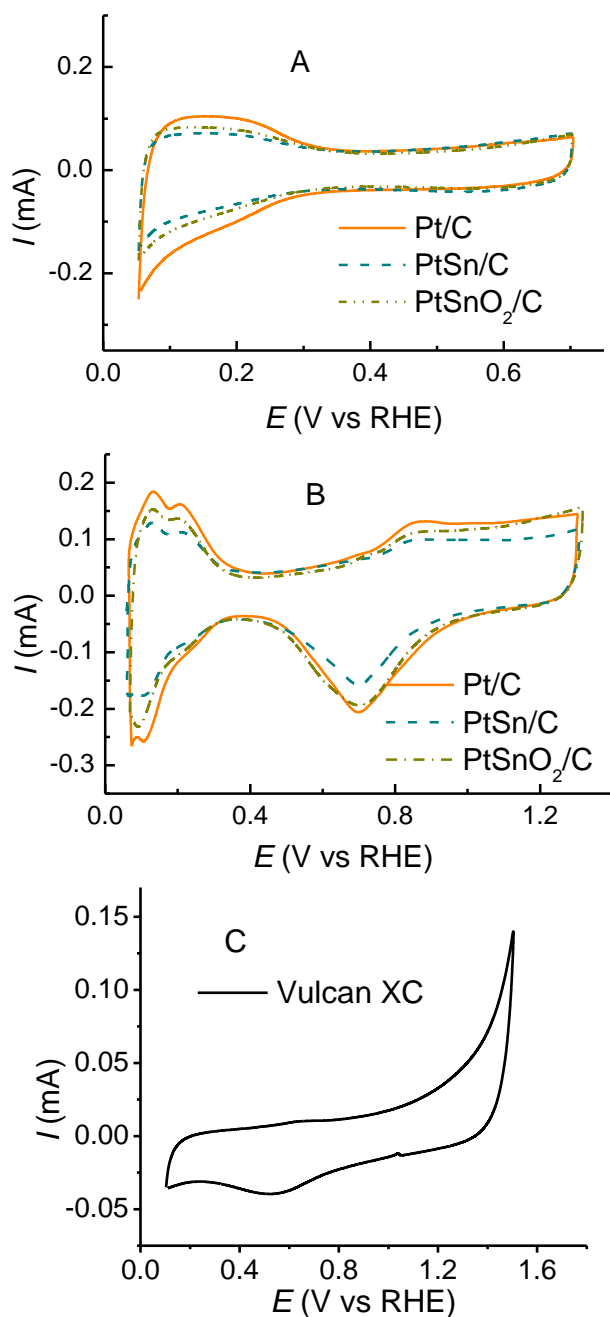


Figure 3. Cyclic voltammograms of (A) as-prepared and (B) oxide annealed Pt/C, PtSn/C and PtSnO₂/C catalysts and (C) cyclic voltammogram Vulcan XC in 0.1 M HClO₄, $\nu = 50$ mV/s.

Fig. 3A shows the comparison of CV curves for all three as-prepared catalysts. The presence of hydrogen adsorption/desorption area can be noticed in potential region from -0.25 V to 0.1 V. As can be seen, this region is shapeless and characteristic peaks that should denote (110) and (100) sites of polycrystalline Pt particles [28] are not recorded. This is due to the adsorption of oxygen and/or carbon species on the catalyst surface during air drying of the suspension. However, upon oxide annealing, as a consequence of oxidation of adsorbed species during cycling at higher potentials (Fig. 3 B) all three

catalysts showed well-defined hydrogen adsorption/desorption region. EASA is calculated from CO_{ads} stripping voltammetry and presented in Table 2.

Table 2. EASA of Pt/C, PtSn/C and PtSnO₂/C catalysts obtained from CO_{ads} oxidation reaction

Catalyst	Pt/C	PtSn/C	PtSnO ₂ /C
EASA for as-prepared (cm ²)	3.4	1.7	2.5
EASA for oxide annealed (cm ²)	2.0	1.3	1.9

* EASA for Pt-Sn catalyst refers only to Pt since CO does not adsorb at Sn [21],

The decrease in EASA is a consequence of morphology changes that occur during potential cycling. It is generally accepted that Pt nanoparticles contain (111) and (100) facets and (110) corner and edges [28]. It is also confirmed by STM analysis that highly under coordinated Pt ad-islands exist on the surface of low index Pt single crystals [29]. In addition, studies at low index Pt single crystals revealed that if they were annealed up to 0.95 V/RHE in HClO₄ solution, diffusion of platinum atoms occur and larger randomly distributed ad-islands were formed [30]. Such description of catalyst surfaces can be applied on our synthesized catalysts as well. Since all the catalysts were treated similarly, the decrease in EASA upon oxide annealing should be the result of similar morphological changes i.e. diffusion of Pt adatoms and growth of surface Pt islands. Alongside with these changes, a few other processes occur. According to Tang et al. [30] stability of Pt nanoparticles is dependent of an applied potential while dissolution of Pt nanoparticle attains by direct electrooxidation of Pt to soluble Pt²⁺. In-situ STM study [31] of Pt nanoparticles under potential cycling treatment revealed that at double-layer potentials, Pt nanocrystals grew rapidly due to Ostwald ripening mechanism in which small islands emitted adatoms that diffused on the surface to larger islands. However, at potentials higher of 1.0 V Pt nanoparticles dissolve and coarsening and growth of Pt also occur. Sugawara and co-workers [32] came to a conclusion that decrease in EASA was consequence of agglomeration of Pt nanoparticles rather than electrochemical Ostwald ripening. The dissolution of platinum becomes significant when the potentials of 1.4 V are reached, but the EASA does not decrease much more than when the potential limit is 1.0 V, and the dissolution of Pt is less. According to Hartl and co-workers [33] potential hold or cycling up to 0.55 V vs RHE does not influence nanoparticles arrangement, but exceeding potential to 1.05 V results in particles migration and their coalescence. Considering all these findings we think that decrease in EASA of our Pt/C catalyst upon oxide annealing is related to the particles agglomeration and to some degree their dissolution.

When PtSn/C catalyst is in question, tin dissolution also contributes to decrease in EASA. The values of EASA for as-prepared PtSn/C are 58% of the EASA values for Pt/C catalyst which agrees well with EDX composition of PtSn/C catalyst. The value for EASA of such treated PtSn/C catalyst surface should approach the value for Pt/C catalyst treated on the similar way since increasing of Pt-like phase starts to occur. However, data analysis from Table 1 reveals only partly dissolution of Sn for oxide annealed surface (EASA for such PtSn/C refers now to 68% of EASA for similarly treated Pt/C) what means that a lot of Sn as stable oxide remain within surface layer. ICP-MS analysis of electrolyte

after cyclization of potentials up to 1.0 V or higher has revealed small amounts of Pt and Sn in the solution.

Since the PtSnO₂/C catalyst has large SnO₂ particles which should be stable at higher potentials, the decrease in EASA is related to platinum agglomeration and dissolution. This catalyst in comparison to PtSn/C is Pt rich and therefore its real surface area is larger both for as-prepared and oxide annealed catalyst.

Oxidation of adsorbed CO

Oxidation of adsorbed CO was carried out not only to determine electrochemically active surface area but also with a purpose of establishing structure-activity relationships for CO tolerance of the examined catalysts surfaces. It is well known that CO poisons Pt surface and impedes H₂O dissociation. Alloying of Sn with Pt improves the rate of CO oxidation despite the fact that the pure Sn does not react with CO [7, 11, 12, 34]. Due to mobility, Pt and Sn atoms separate during the oxidation of CO to the Pt and Sn-oxide domains [35]. Adsorbed CO remains on Pt while oxygen stays on Sn. Stripping curves for CO_{ads} from all Pt/C, PtSn/C and PtSnO₂/C surfaces are presented in Fig 4.

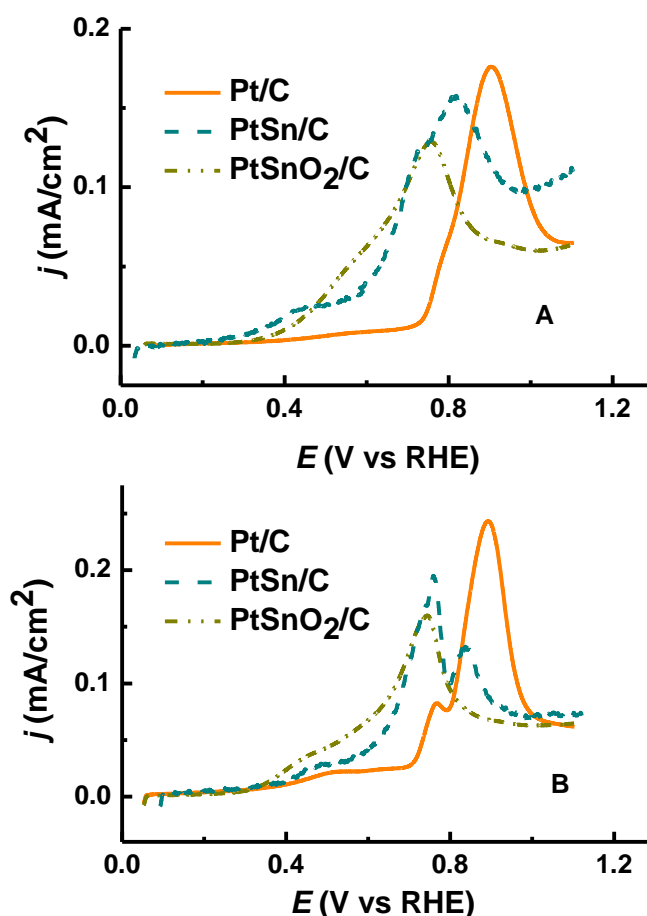


Figure 4. CO_{ads} stripping curves for as-prepared (A) and oxide annealed (B) Pt/C, PtSn/C and PtSnO₂/C catalysts in 0.1 M HClO₄, $v = 50$ mV/s.

The CO_{ads} stripping curve for Pt/C surface shows sharp peak at ~ 0.55 V/SCE and shoulder at ~ 0.45 V/SCE while the onset potential depending on the surface morphology. At oxide annealed Pt/C catalyst CO_{ads} oxidation starts at lower potential in comparison to as-prepared. CO oxidation at Pt follows Langmuir-Hinshelwood mechanism which points that oxidative removal of CO_{ads} is strongly dependent of surface defects since they adsorbed active OH [36-38]. The CO_{ads} stripping curve for oxide annealed Pt/C surface shows two peaks related with two different settlements of CO and two kinds of OH [34] and have been recorded at agglomerated Pt particles [38, 39]. We assume that the same goes for our oxide annealed Pt/C catalyst. The oxidative treatment leads to particles agglomeration and formation of defects in form of steps and grain boundaries. Smaller particles have less numbers of defects and thus higher CO binding [39]. When oxide annealed Pt/C catalyst is in question (Fig. 4B) the peak at lower potential indicated CO_{ads} oxidation at agglomerated particles while the peak at higher potential indicate CO_{ads} oxidation at single particles.

CO_{ads} oxidation at as-prepared and oxide annealed PtSn/C catalysts shows the negatively shifted onset potential for more than 0.4 V compared to Pt/C catalysts (Fig. 4A and B). At these surfaces CO_{ads} oxidize with two peaks: first at more negative potential is correlated with Pt-Sn like phase and the second one is correlated with Pt-like phase.

At the oxide annealed surface both peaks are well defined since dissolution of alloyed Sn leads to increase of the Pt-like phase. The surface of as-prepared PtSn/C catalyst should contain SnO₂ and Pt₃Sn particles while oxide annealed PtSn/C only SnO₂. Their increased activity especially at lower potentials indicates that SnO₂ particles are closely connected with Pt [9, 35, 40, 41]. The presence of alloyed Sn in as-prepared PtSn/C catalyst with the appreciable difference in electronegativity of Sn and Pt, could withdraw Pt electrons and induce charge transfer from Sn to Pt in Pt-Sn system [42]. Thus a weaker adsorption of CO and OH is the result of increased electron density of Pt-sites. Numerous spectroscopic and theoretical predictions confirmed that Sn reduces the adsorption of CO on Pt (ligand effect) [16, 39]. On the other hand, Sn sites prefer OH adsorption [29] at the same potential where starts CO oxidation [42-46].

The CO_{ads} stripping curves for as-prepared and oxide annealed PtSnO₂/C catalysts shows only one peak with a maximum that correlates to Pt-Sn like phase (Fig. 4A and B). The peak for Pt-like phase are not present probably as a consequence of very close association SnO₂ and Pt particles.

Methanol oxidation

The potentiodynamic measurements of the as-prepared and oxide annealed Pt/C, PtSn/C and PtSnO₂/C catalysts for methanol oxidation are presented in Fig. 5A and B respectively.

The reaction is enhanced at PtSn/C and PtSnO₂/C catalysts with about two times higher currents and onset potential starts ~100 mV earlier at *ap* and ~50 mV at oxide annealed surfaces in comparison to Pt/C. Slightly better activity for PtSn/C catalyst, either as-prepared or oxide annealed can be seen from the voltamograms. Higher currents at as-prepared PtSn/C in comparison to as-prepared PtSnO₂/C are related with alloyed Sn and its electronic effect (Fig.5A). However all three catalysts are more active after oxide annealing.

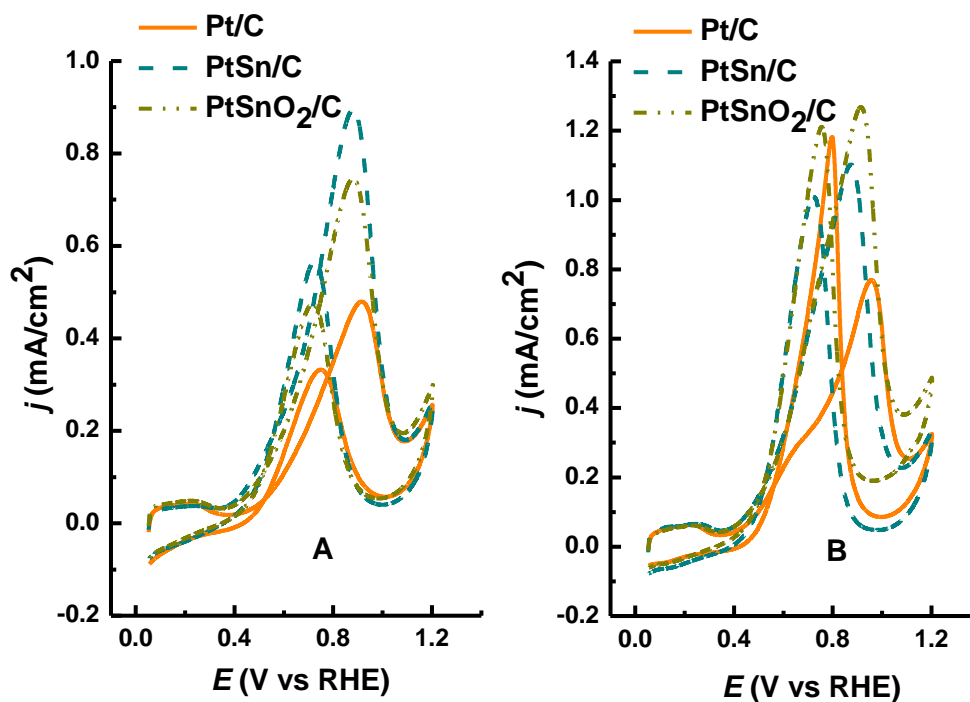


Figure 5. Cyclic voltammograms recorded in 0.5 M CH₃OH + 0.1 M HClO₄ at as-prepared (A) and oxide annealed (B) Pt/C, PtSn/C and PtSnO₂/C catalysts, $v = 50$ mV/s.

As explained in the previous section, the activity for the oxidation of CO_{ads} is higher at oxide annealed catalysts. Therefore both Pt-Sn catalysts as well as Pt/C are more active for methanol oxidation when they are electrochemically treated than as-prepared [45,46]. Considering the activity for the oxidation of CO_{ads} at Pt-Sn catalysts when a significant fraction of adsorbed CO is oxidized at low potentials in a first cycle, one could expect better activity for methanol oxidation especially at lower potentials. However, contrary to direct CO adsorption, multiple Pt atom sites are needed for methanol adsorption and dehydrogenation. Due to crumpling of CO molecules on Pt sites and their repulsive interaction, their weak adsorption causes that oxidation of CO_{ads} for PtSn/C catalyst begins at lower potentials, what is not the case when methanol is in question [47].

Analyzing the CVs from Fig.5 it can be noticed that for all catalysts and surfaces except oxide annealed Pt/C, peak current in anodic (forward) scan is higher than in cathodic (reverse) scan. Anodic scanning leads to the formation of intermediates, while during cathodic scanning they are removed. For that reason, the peak currents ratio in forward and backward scan (j_f/j_b) can define the catalyst tolerance to carbonaceous species [48-50]. As a matter of fact, a higher ratio suggests that a lesser amount of unwanted CO molecules blocks the catalyst surface. This ratio is highest for PtSn/C catalysts both in a form of as-prepared and at oxide annealed surfaces and suggests higher resistance versus poisoning intermediate products. All values for j_f/j_b ratio are summarized in Table 3.

Table 3. The j_f/j_b ratio for Pt/C, PtSn/C and PtSnO₂/C catalysts for the methanol oxidation

Catalyst	Pt/C	PtSn/C	PtSnO ₂ /C
j_f/j_b for as-prepared	1.45	1.56	1.52
j_f/j_b for oxide annealed	0.65	1.094	1.04

Electrocatalytic stability of the catalysts was examined by prolonged cycling as well as by chronoamperometric measurements in HClO₄/CH₃OH solution. Long-term stability for as-prepared and oxide annealed Pt/C, PtSn/C and PtSnO₂/C catalysts is displayed in Fig.6.

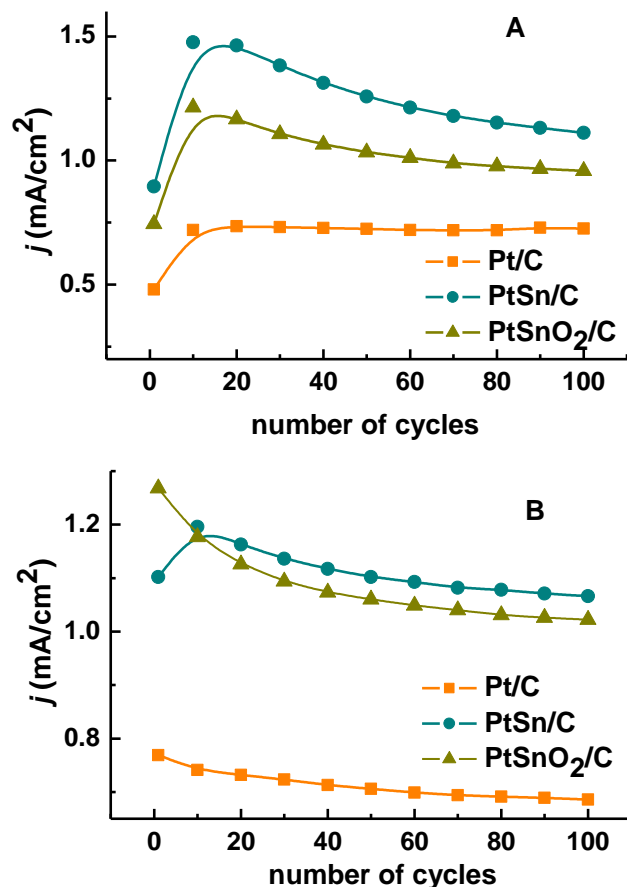


Figure 6. Long-term stability for as-prepared (A) and oxide annealed (B) Pt/C, PtSn/C and PtSnO₂/C in 0.1 M HClO₄ + 0.5 M CH₃OH (current values are at 0.4 V, $v = 50$ mV/s).

For as-prepared catalysts from long-term stability test (Fig. 6A), currents are increasing during first 20 cycles and then start to decrease. The decline in currents is most prominent at PtSn/C and least at Pt/C. However, during stability test at oxide annealed catalysts it can be observed that after the initial faster decline which happens in the first 20-30 cycles, the currents continue to decline very slowly during further cyclization (Fig. 6B). We assume that the increase in currents for as-prepared catalysts is due to the morphology changes during cyclization which is approaching the one obtained after oxide annealed. As all catalysts are more active if oxide annealed, the currents are increasing.

Since during this process Sn is dissolving from the surface changes in currents are most pronounced for PtSn/C and then for PtSnO₂/C.

In order to get better insight in to morphology changes during long-term stability tests, we performed stripping of CO_{ads} after finishing 100 cycles at all three catalysts (Fig. 7).

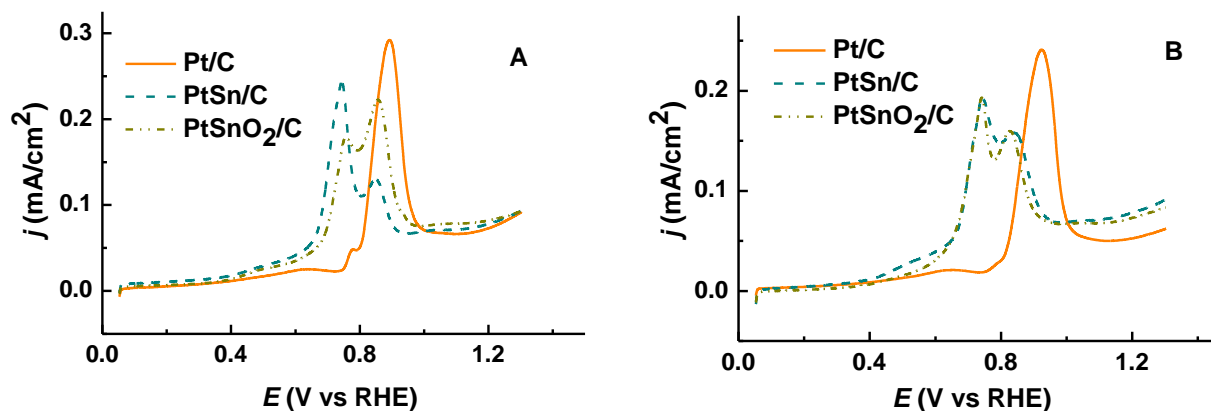


Figure 7. CO_{ads} stripping curves for as-prepared (A) and oxide annealed (B) catalysts for Pt/C, PtSn/C and PtSnO₂/C catalysts after stability tests in 0.1 M HClO₄, $v = 50$ mV/s.

The stripping curves for all three catalysts revealed impact of electrode pre-treatment by potential cycling on morphology changes of all surfaces. Namely, oxide annealed i.e. pre-treated electrodes underwent significantly less changes during methanol oxidation due to dissolution and redeposition of Pt. CO stripping curves after the test are practically the same as those before the test except for PtSnO₂/C catalysts for which two peaks are recorded after prolonged methanol oxidation signifying Pt-Sn like phase and Pt phase (Figs. 4b and 7b respectively). On the other side, stripping curves of CO_{ads} for all untreated as-prepared catalyst after stability test in comparison to those before the test (Figs, 7a and 4a respectively), indicate notably changed surfaces. The curves for as-prepared catalysts after the test display features similar to those of stripping curves for oxide annealed surfaces both before and after the stability test i.e. two peaks for PtSn/C and PtSnO₂/C and additional small peak (shoulder) for Pt/C catalyst (Figs, 7a, 4b and 7b respectively). Therefore morphological changes during methanol oxidation at as-prepared catalysts are related to particles agglomeration and dissolution of Pt and Sn.

All of these experiments performed by cyclic voltammetry reveal only similarity in activity, stability and poisoning tolerance of the catalysts containing Sn with slight advantage of PtSn/C in comparison to PtSnO₂/C. This advantage is corroborated by additional chronoamperometric experiments (Fig. 8).

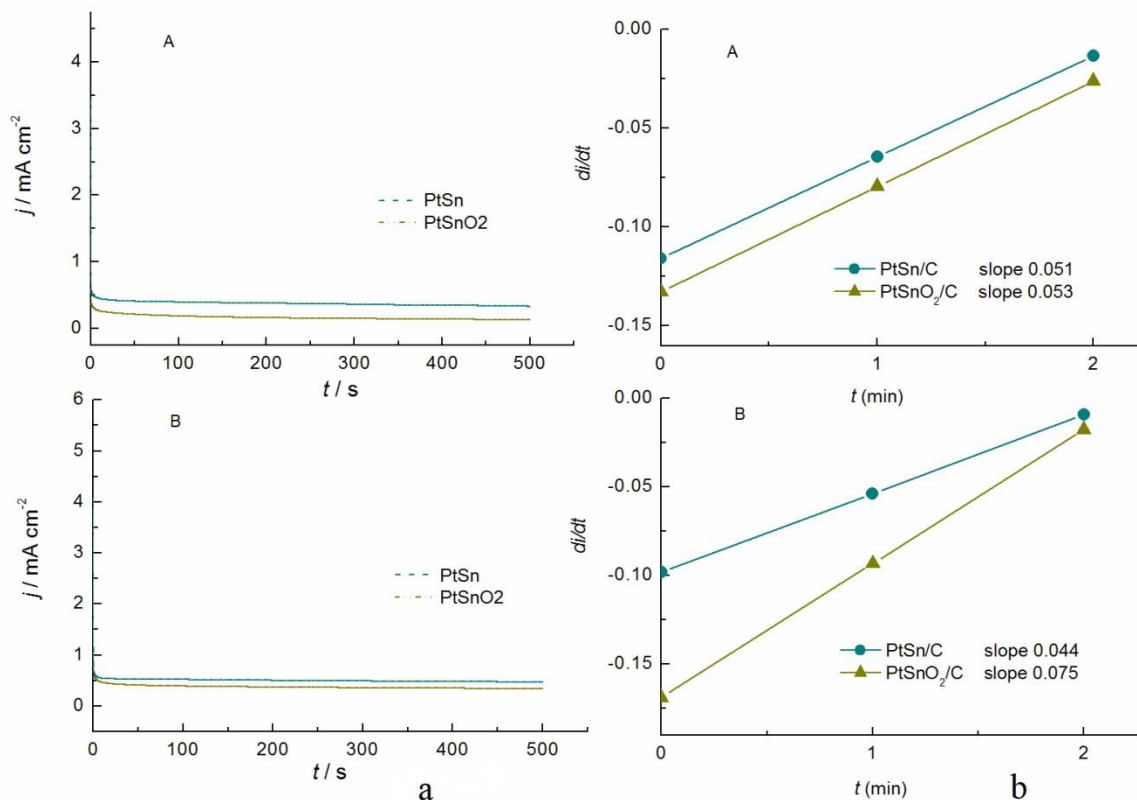


Figure 8. a) Chronoamperometric curves for the oxidation of 0.5 M CH₃OH at as-prepared (A) and oxide annealed (B) Pt/C, PtSn/C and PtSnO₂/C catalysts in 0.1 M HClO₄ at 0.2 V vs SCE; b) di/dt versus time plots (from $t = 0$ to $t = 120$ s) as-prepared (A) and oxide annealed (B) Pt/C, PtSn/C and PtSnO₂/C catalysts.

Both catalysts demonstrate similar behavior which is consistent with potentiodynamic measurements (Fig. 5). The values of current for both PtSn/C surfaces are higher than for PtSnO₂/C catalysts. That proves the lower poisoning of PtSn/C than PtSnO₂/C (Fig. 9a). Less poisoning of PtSn/C is also visible from di/dt plots (Fig.9b). A lower slope value indicates that initial poisoning of the surface is also lower. [51]. Therefore it seems that alloyed Sn and its electronic effect facilitate lower poisoning of the catalyst better than SnO₂.

4. CONCLUSION

Two type of Pt/Sn carbon supported catalyst have been successfully synthesized by microwave assisted polyol procedure. PtSn/C catalyst was made of Pt, Pt₃Sn alloy and small SnO₂ particles while PtSnO₂/C catalysts was made of Pt with larger SnO₂ particles. TEM analysis of all catalysts showed small particles of rather similar size between 2 and 3 nm. The results from cyclic voltammetry experiments showed improved catalytic activities for methanol oxidation reaction as well improved tolerance to CO, after adding of Sn, regardless of whether tin is present in alloyed or oxide form.

However PtSn/C shows slight advantage in activity regarding to PtSnO₂/C catalyst. It can be concluded that electronic effect of alloyed Sn is more dominant than Sn in form of oxide.

ACKNOWLEDGEMENTS

This work was financially supported by the Ministry of Education, Science and Technological Development of the republic of Serbia (Grant No. 451-03-68/2020-14/200026).

References

1. S. Arico, S. Srinivasan, V. Antonucci, *Fuel Cells* 1 (2001) 133.
2. H. Liu, C. Song, L. Zhang, J. Zhang, H. Wang, D. P. Wilkinson, *J. Power Sources*, 155 (2006) 95.
3. G. Garcia, V. Baglio, A. Stassi, E. Pastor, V. Antonucci, A. S. Aricò, *J Solid State Electrochem*, 11 (2007) 1229.
4. Y. Hu, A. Zhu, Q. Zhang, Q. Liu, *Int. J. Hydrogen Energy*, 41 (2016) 11359.
5. H. Su, T. H. Chen, *Chin. Chem. Lett.*, 27 (2016) 1083.
6. N. R. Mathe, M. R. Scriba, N. J. Coville, *Int. J. Hydrogen Energy*, 39 (2014) 18871.
7. J. Zeng, J. Yang, J. Y Lee, W. Zuou, *J. Phys. Chem. B*, 110 (2006) 24606.
8. M. Arenz, V. Stamenković, B. B. Blizanac, K. J. Mayrhofer, N. M. Marković, P. N. Ross, *J. Catalysis*, 232 (2005) 402.
9. Z. Liu, G. S. Jackson, B. W. Eichhorn, *Angew. Chem.*, 49 (2010) 3173.
10. A. K. Shukla, A. S. Arico, K. M. El-Khatib, H. Kim, P. L. Antonucci, V. Antonucci, *Appl. Surf. Sci.*, 137 (1999) 20.
11. M. Zhu, G. Sun, Q. Xin, *Electrochim. Acta*, 54 (2009) 1511.
12. M. E. Gallager, C. A. Lucas, V. Stamenković, N. M. Marković, P. N. Ross, *Surface Science*, 544 (2003) L729.
13. Y. Jagnet, D. Loffreda, C. Dupont, F. Delbecq, E. Ehret, F. J. C. Aires, B. S. Mun, F. A. Akgul, Z. Liu, *J. Phys. Chem. Lett.*, 3 (2012) 3707.
14. P. Zhang, S. Y. Huang, B. N. Popov, *J. Electrochem. Soc.*, 157 (2010) B1163.
15. S. Q. Song, W. J. Zhou, Z. H. Zhou, L. H. Jiang, G. Q. Suna, Q. Xina, V. Leontidis, S. Kontou, P. Tsiakaras, *Int. J. Hydrogen Energy*, 30 (2005) 995.
16. S. Stevanović, D. Tripković, J. Rogan, K. Popović, J. Lović, A. Tripković, V. M. Jovanović, *J. Solid State Electrochem.*, 16 (2012) 3147.
17. S. Stevanović, D. Tripković, V. Tripković, D. Minić, A. Gavrilović, A. Tripković, V. M. Jovanović, *J. Phys. Chem. C*, 118 (2014) 278.
18. Bruker AXS, TOPAS V3. General profile and structure analysis software for powder diffraction data, Karlsruhe, 2005.
19. V. M. Goldschmidt, T. Land, *J. Iron Steel Inst. London*, 155 (1947) 221.
20. R. Harris, M. Norman, A. W. Bryant, *J. Less-Common Met.*, 16 (1968) 427.
21. P. Durussel, R. Massara, P. Feschotte, *J. Alloys Compds.*, 215 (1994) 175.
22. Haines, J. M. Leger, *Phys. Rev. B: Condens. Matter. Mater. Phys.*, 55 (1997) 11144.
23. H. P. Klug, L. E. Alexander, *X ray diffraction procedures 2nd ed.* Wily, (1974) New York.
24. Z. Liu, B. Guo, L. Hong, T. H. Lim, *Electrochem. Commun.*, 8 (2006) 83.
25. Z. Liu, L. Hong, S. W. Tay, *Mater. Chem. Phys.*, 105 (2007) 222.
26. E. Lee, A. Murthy, A. Manthiram, *J. Electroanal. Chem.*, 659 (2011) 168.
27. Solla-Gullon, P. Rodriguez, E. Herrero, A. Aldaz, J. M. Feliu, *Phys. Chem. Chem. Phys.*, 10 (2008) 359.
28. T. E. Shubina, M. T. Koper, *Electrochim Acta*, 47 (2002) 3621.

29. D. Strmcnik, D. Tripković, D. Vliet, K. C. Chang, V. Komanicky, H. You, G. Karapetrov, J. Greeley, V. Stamenković, N. M. Marković, *J. American Chem. Soc.*, 130 (2008) 15332.
30. Tang, B. Han, K. Persson, C. Friesen, T. He, K. Sieradzki, G. Ceder, *J. American Chem. Soc.*, 132 (2010) 596.
31. Q. Xu, E. Kreidler, D. O. Wipf, T. He, *J. Electrochem. Soc.*, 155 (2008) B228.
32. Y. Sugawara, A. P. Yadav, A. Nishikata, T. Tsuru, *J. Electroanal. Chem.*, 662 (2011) 379.
33. K. Hartl, M. Nesselberger, K. J. J. Mayrhofer, S. Kunz, F. F. Schweinberger, G. H. Kwon, M. Hanzlik, U. Heiz, M. Arenz, *Electrochim. Acta*, 56 (2010) 810.
34. Dupont, Y. Jugnet, F. Delbecq, D. Loffreda, *J. Catal.* **273** (2010) 211
35. W. D. Michalak, J. M. Krier, S. Alayoglu, J. Y. Shin, K. An, K. Komvopoulos, Z. Liu, G. A. Somorjai, *J. Catal.*, 312 (2014) 17.
36. Arenz, K. J. J. Mayrhofer, V. Stamenković, B. B. Blizanac, T. Tomoyuki, P. N. Ross, N. M. Marković, *J. Am. Chem. Soc.*, 127 (2005) 6819.
37. A. Lopez-Cudero, J. Solla-Gullon, E. Herrero, A. Aldaz, J. M. Feliu, *J. Electroanal. Chem.*, 644 (2010), 117.
38. F. Maillard, S. Schreier, M. Hanzlik, E. R. Savinova, S. Weinkauff, U. Stimming, *Phys. Chem. Chem. Phys.*, 7 (2005) 385.
39. V. Radmilovic, T. J. Richardson, S. J. Chen, P. N. Ross, *J. Catalysis*, 232 (2005) 199.
40. T. Matsui, K. Fujiwara, T. Okanishi, R. Kikuchi, T. Takeguchi, K. Eguchi, *J. Power Sources*, 155 (2006) 152.
41. Y. Lin, S. Zhang, S. Yan, G. Liu, *Electrochim. Acta*, 66 (2012) 1.
42. E. Hayden, M. E. Rendall, O. South, *J. Am. Chem. Soc.*, 125 (2003) 7738.
43. P. N. Ross, *J. Vac. Sci. Technol. A*, 10 (1992) 2546.
44. T. Iwasita, *Electrochim. Acta*, 47 (2002) 3663.
45. B. Beden, F. Hahn, C. Lamy, J. M. Leger, N. R. Tacconi, R. O. Lezna, A. J. Arvia, *J. Electroanal. Chem.*, 261 (1989) 401.
46. M. Marković, P. N. Ross, *Surf. Sci. Rep.*, 45 (2002) 117.
47. K. Wang, A. Gasteiger, N. M. Marković, P. N. Ross, *Electrochim. Acta*, 41 (1996) 2587.
48. Y. Zhao, L. Chen, Y. Song, Y. Meng, *Int. J. Electrochem. Sci.*, 13 (2018) 7370.
49. L. J. Zhang, D. G. Xia, *Appl. Surf. Sci.*, 252 (2006) 2191.
50. J. Lović, S. Stevanović, *Int. J. Electrochem. Sci.*, 15 (2020) 3761.
51. F. Delime, J. M. Léger, C. Lamy, *J. Appl. Electrochem.*, 28 (1998) 27.